A new concept of Monte Carlo kinetics parameter calculation using complex-valued perturbation

Toshihiro Yamamoto[a,*]

Hiroki Sakamoto[b]

[a]*Research Reactor Institute, Kyoto University, 2 Asashiro Nishi, Kumatori-cho, Sennan-gun, Osaka, 590-0494, Japan*

[b]*Transnuclear Tokyo, Ltd., 1-18-16, Shinbashi, Minato-ku, Tokyo, 105-0004, Japan*

Abstract

A new Monte Carlo method to calculate two types of kinetics parameters, the effective delayed neutron fraction (β_{eff}) and the prompt neutron generation time (Λ), is proposed in this paper. The new method uses perturbation techniques in which extra delayed neutrons or a fictitious $1/v$ absorber is added to the unperturbed system to calculate the β_{eff} or Λ, respectively. In the new method, the perturbation is added as a complex-valued perturbation. This paper conjectures that the change in the eigenvalue due to the perturbation is accurately approximated by the imaginary part of the eigenvalue of the complex-valued perturbed equation. The conjecture is corroborated by certain numerical tests presented in this paper. A Monte Carlo calculation algorithm is established to solve the complex-valued perturbed eigenvalue equation. One single Monte Carlo calculation to solve the complex-valued eigenvalue equation yields highly accurate approximations of the exact kinetics parameters with much less computational costs compared with the previously proposed method that uses multiple Monte Carlo

* Corresponding author. Tel: +81 72 451 2414; Fax: +81 72 451 2658
E-mail address: toshihiro.yamamoto223@gmail.com (T. Yamamoto)

runs.

Keywords: Monte Carlo, kinetics parameter, perturbation theory, generation time, delayed neutron

1. Introduction

Although the continuous-energy Monte Carlo method is widely considered a versatile calculation tool for particle transport problems, problems remain that the Monte Carlo method cannot properly handle. The perturbation calculation and the calculation of kinetics parameters, such as the effective delayed neutron fraction (β_{eff}) and the prompt neutron generation time (Λ), are among the examples of problems that must be solved. The difficulties in these calculations stem from the difficulties in the calculations of the adjoint flux in a continuous-energy scheme. These difficulties are remaining problems that must be overcome to expand the capability of the Monte Carlo method.

Many studies have been performed on the Monte Carlo method for calculating kinetics parameters. A method proposed by Meulekamp and van der Mark (2006) and by Nauchi and Kameyama (2005) approximates the adjoint function (i.e., the importance of a neutron) with the probability that a neutron causes fission in the next generation. Although this method is an approximate estimate for a true adjoint function (Nagaya et al., 2010), the kinetics parameters can be obtained using the forward calculation without performing the backward calculation. The approximation was recently improved by introducing the concept of “iterated fission probability (IFP)”. Many papers have been published concerning the works that use the IFP method (Raskach and Blyskavka, 2010; Shim et al., 2010; Nauchi and Kameyama, 2010;

Kiedrowski et al., 2011; Leppänen et al., 2014). The IFP method extends the fission chains up to several generations in the future. A similar concept has been proposed by Feghhi et al. (2008). This concept corresponds to a method named "integrated fission probability" by Bécares et al. (2014). These methods, IFP and "integrated fission probability", have been reviewed and compared by Bécares et al. (2014).

Another approach for calculating kinetics parameters uses the perturbation theory. For calculating β_{eff}, a fictitious change in the number of delayed neutrons is added to a system as a perturbation (Nagaya and Mori, 2011). Then, we can obtain an approximate β_{eff} of the unperturbed system from the change in k_{eff} caused by the perturbation. Similarly, for calculating the Λ, a $1/v$-absorber is uniformly added to a system as a perturbation (Verboomen et al., 2006). An approximate Λ is estimated from the reactivity caused by the $1/v$-absorber. To obtain an accurate kinetics parameter, the perturbation must be small. However, the Monte Carlo method has difficulties in calculating the small difference in k_{eff}. Nagaya and Mori (2011) developed a Monte Carlo technique for calculating an exact β_{eff} by taking the infinitesimally small limit of the perturbation using the differential operator sampling technique.

The present paper proposes a new method of calculating kinetics parameters based on perturbation methods. The new method introduces a complex-valued perturbation into an ordinary real-valued eigenvalue equation. The change in k_{eff} is accurately (but not exactly) provided by the imaginary part of the complex-valued eigenvalue of the perturbed equation. In the sections that follow, the theory and numerical examples are presented.

2. Monte Carlo Calculation of the β_{eff}

2.1. Calculation technique of the complex-valued perturbation method

This section presents how the effective delayed neutron fraction (β_{eff}) is calculated by the perturbation theory based on the method by Nagaya and Mori (2011). Then, a new method in which a complex-valued perturbation is introduced to a transport eigenvalue equation is explained. In (Nagaya and Mori, 2011), the β_{eff} is obtained by the following equation:

$$\beta_{eff} = \lim_{a \to 0} \frac{1}{k(0)} \frac{k(a) - k(0)}{a}, \tag{1}$$

where $k(0)$ is the effective multiplication factor of an unperturbed eigenvalue equation, and $k(a)$ is the perturbed effective multiplication factor. The unperturbed eigenvalue equation based on the transport theory is as follows:

$$\mathbf{H}\phi(\mathbf{r}, \mathbf{\Omega}, E) = \frac{1}{k(0)} S_f(\mathbf{r}, \mathbf{\Omega}, E), \tag{2}$$

where

$$\begin{aligned} &\mathbf{H}\phi(\mathbf{r}, \mathbf{\Omega}, E) \\ &\equiv \mathbf{\Omega} \cdot \nabla \phi(\mathbf{r}, \mathbf{\Omega}, E) + \Sigma_t(\mathbf{r}, E)\phi(\mathbf{r}, \mathbf{\Omega}, E) \\ &- \int_{4\pi} d\mathbf{\Omega}' \int dE' \Sigma_s(\mathbf{r}, \mathbf{\Omega}' \to \mathbf{\Omega}, E' \to E)\phi(\mathbf{r}, \mathbf{\Omega}', E'), \end{aligned} \tag{3}$$

$$S_f(\mathbf{r}, \mathbf{\Omega}, E) = S_f^p(\mathbf{r}, \mathbf{\Omega}, E) + \sum_j S_{f,j}^d(\mathbf{r}, \mathbf{\Omega}, E), \tag{4}$$

$$S_f^p(\mathbf{r}, \mathbf{\Omega}, E) = \sum_m \frac{\chi_m^p(E)}{4\pi} \int_{4\pi} d\mathbf{\Omega}' \int dE' \nu_m^p(E') \Sigma_{f,m}(\mathbf{r}, E')\phi(\mathbf{r}, \mathbf{\Omega}', E'), \tag{5}$$

$$S_{f,j}^d(\mathbf{r}, \mathbf{\Omega}, E) = \sum_m \frac{\chi_{m,j}^d(E)}{4\pi} \int_{4\pi} d\mathbf{\Omega}' \int dE' \nu_{m,j}^d(E') \Sigma_{f,m}(\mathbf{r}, E')\phi(\mathbf{r}, \mathbf{\Omega}', E'), \tag{6}$$

$\phi(\mathbf{r}, \mathbf{\Omega}, E) =$ the neutron flux at position $\mathbf{r}$ with energy E and direction $\mathbf{\Omega}$, $\Sigma_t =$ the

macroscopic total cross section, $\Sigma_s =$ the macroscopic scattering cross section, $\Sigma_{f,m} =$ the macroscopic fission cross section of nuclide *m*, $\chi_m^p(E) =$ the prompt neutron spectrum of nuclide *m*, $\chi_{m,j}^d(E) =$ the delayed neutron spectrum of nuclide *m* and delayed neutron family *j*, $\nu_m^p(E) =$ the number of prompt neutrons per fission of nuclide *m*, and $\nu_{m,j}^d(E) =$ the number of delayed neutrons per fission of nuclide *m* and delayed neutron family *j*. The perturbed eigenvalue, $k(a)$, in Eq. (1) is the eigenvalue of the perturbed eigenvalue equation, as shown below:

$$\mathbf{H}\phi(\mathbf{r},\mathbf{\Omega},E;a) = \frac{1}{k(a)} S_f(\mathbf{r},\mathbf{\Omega},E;a), \tag{7}$$

where

$$S_f(\mathbf{r},\mathbf{\Omega},E;a) = S_f^p(\mathbf{r},\mathbf{\Omega},E;a) + (1+a)\sum_j S_{f,j}^d(\mathbf{r},\mathbf{\Omega},E;a), \tag{8}$$

$$S_f^p(\mathbf{r},\mathbf{\Omega},E;a) = \sum_m \frac{\chi_m^p(E)}{4\pi} \int_{4\pi} d\mathbf{\Omega}' \int dE' \nu_m^p(E') \Sigma_{f,m}(\mathbf{r},E') \phi(\mathbf{r},\mathbf{\Omega}',E';a), \tag{9}$$

$$S_{f,j}^d(\mathbf{r},\mathbf{\Omega},E;a) = \sum_m \frac{\chi_{m,j}^d(E)}{4\pi} \int_{4\pi} d\mathbf{\Omega}' \int dE' \nu_{m,j}^d(E') \Sigma_{f,m}(\mathbf{r},E') \phi(\mathbf{r},\mathbf{\Omega}',E';a). \tag{10}$$

The adjoint equation for the unperturbed system is as follows:

$$\mathbf{H}^*\phi^*(\mathbf{r},\mathbf{\Omega},E) = \frac{1}{k(0)} S_f^*(\mathbf{r},\mathbf{\Omega},E), \tag{11}$$

where

$$\begin{aligned} &\mathbf{H}^*\phi^*(\mathbf{r},\mathbf{\Omega},E) \\ &\equiv -\mathbf{\Omega}\cdot\nabla\phi^*(\mathbf{r},\mathbf{\Omega},E) + \Sigma_t(\mathbf{r},E)\phi^*(\mathbf{r},\mathbf{\Omega},E) \\ &- \int_{4\pi} d\mathbf{\Omega}' \int dE' \Sigma_s(\mathbf{r},\mathbf{\Omega}\to\mathbf{\Omega}',E\to E')\phi^*(\mathbf{r},\mathbf{\Omega}',E'), \end{aligned} \tag{12}$$

$$S_f^*(\mathbf{r},\mathbf{\Omega},E) = S_f^{*p}(\mathbf{r},\mathbf{\Omega},E) + \sum_j S_{f,j}^{*d}(\mathbf{r},\mathbf{\Omega},E), \tag{13}$$

$$S_f^{*p}(\mathbf{r},\mathbf{\Omega},E;a)=\sum_m \frac{\nu_m^p(E)\Sigma_{f,m}(\mathbf{r},E)}{4\pi}\int_{4\pi} d\mathbf{\Omega}'\int dE'\,\chi_m^p(E')\phi^*(\mathbf{r},\mathbf{\Omega}',E';a), \quad (14)$$

$$S_{f,j}^{*d}(\mathbf{r},\mathbf{\Omega},E;a)=\sum_m \frac{\nu_{m,j}^d(E)\Sigma_{f,m}(\mathbf{r},E)}{4\pi}\int_{4\pi} d\mathbf{\Omega}'\int dE'\,\chi_{m,j}^d(E')\phi^*(\mathbf{r},\mathbf{\Omega}',E';a). \quad (15)$$

Using Eqs. (7) and (11), we obtain the following equation:

$$\frac{1}{k(0)}\frac{k(a)-k(0)}{a}=\frac{\sum_j\left\langle\phi^*(\mathbf{r},\mathbf{\Omega},E)S_{f,j}^d(\mathbf{r},\mathbf{\Omega},E;a)\right\rangle}{\left\langle\phi^*(\mathbf{r},\mathbf{\Omega},E)\left[S_f^p(\mathbf{r},\mathbf{\Omega},E;a)+\sum_j S_{f,j}^d(\mathbf{r},\mathbf{\Omega},E;a)\right]\right\rangle}, \quad (16)$$

where the angle brackets denote integration over all phase space. Thus, the limit of Eq. (16) as a approaches zero becomes the following equation:

$$\beta_{eff}=\frac{\sum_j\left\langle\phi^*(\mathbf{r},\mathbf{\Omega},E)S_{f,j}^d(\mathbf{r},\mathbf{\Omega},E)\right\rangle}{\left\langle\phi^*(\mathbf{r},\mathbf{\Omega},E)\left[S_f^p(\mathbf{r},\mathbf{\Omega},E)+\sum_j S_{f,j}^d(\mathbf{r},\mathbf{\Omega},E)\right]\right\rangle}. \quad (17)$$

Eq. (1) gives an exact β_{eff} if the limit as a approaches zero can be exactly obtained. In (Nagaya and Mori, 2011), the limit is taken by the introduction of the differential operator sampling technique.

An approximate β_{eff} can be calculated using the left-hand side of Eq. (16) for a non-zero a, as shown below:

$$\beta_{eff}\approx\frac{1}{k(0)}\frac{k(a)-k(0)}{a}. \quad (18)$$

A Monte Carlo calculation of the β_{eff} using Eq. (18) would require small statistical uncertainties for two independent Monte Carlo calculations. Calculating an accurate β_{eff} requires that the perturbation parameter a be small enough to keep the perturbation within the range of linearity. As a becomes smaller, the computational cost for calculating an accurate β_{eff} increases. However, if the linearity is kept for a larger a, then

the requirement for the small uncertainties is relaxed, and the computational cost may be reduced. This topic is mentioned later in this paper.

The method of Eq. (18) is similar to the so-called "prompt method" (Bretscher, 1997; Meulekamp and van der Marck, 2006; Carta et al., 2011). The "prompt method" approximates the β_{eff} as follows:

$$\beta_{eff} \approx 1 - \frac{k_p}{k(0)}, \tag{19}$$

where k_p is the eigenvalue of Eq. (2) calculated without delayed neutrons (i.e., $\nu^d_{m,j} = 0$). The "prompt method" is identical to Eq. (18) when $a = -1$. The difference between k_p and $k(0)$ is less than or comparable to 0.008. In a fuel composed of ^{239}Pu, the difference is much smaller. The computational cost of the "prompt method" may be prohibitively large for obtaining the β_{eff} within an accuracy of pcm order. Although the degree of perturbation in Eq. (18) can be arbitrarily chosen and expanded, the perturbation in the "prompt method" is always fixed.

The present paper proposes a new method in which a complex-valued perturbation is added to the unperturbed eigenvalue equation, Eq. (2), as shown below:

$$\mathbf{H}\tilde{\phi}(\mathbf{r},\mathbf{\Omega},E;a) = \frac{1}{\tilde{k}(a)}\left(\tilde{S}^p_f(\mathbf{r},\mathbf{\Omega},E;a) + (1+a\,i)\sum_j \tilde{S}^d_{f,j}(\mathbf{r},\mathbf{\Omega},E;a) \right), \tag{20}$$

where $i = \sqrt{-1}$, and the tilde denotes a complex-valued quantity. The authors of the present paper pose a conjecture that the imaginary part of the complex-valued eigenvalue $\tilde{k}(a)$ (i.e., $\mathrm{Im}[\tilde{k}(a)]$) represents an extremely close approximation of the difference in k ($= k(a) - k(0)$) caused by the perturbation. The real part of $\tilde{k}(a)$ (i.e., $\mathrm{Re}[\tilde{k}(a)]$) may represent the unperturbed eigenvalue, $k(0)$. The mathematical interpretation of this conjecture cannot be presented at this stage. The conjecture is to be corroborated by scrutinizing the results of some numerical tests shown below.

The advantage of this method is that the difference in k can be obtained by one single eigenvalue calculation. The statistical uncertainty of $\mathrm{Im}[\tilde{k}(a)]$ entailed by the Monte Carlo method is expected to be small, with a reasonable computational cost. Thus, the accuracy of the β_{eff} calculated using this newly proposed method may be comparable to that calculated using other methods, such as deterministic methods or other Monte Carlo methods (e.g., IFP and Nagaya's method).

2.2. Verification by a deterministic method

Before applying the new method to the Monte Carlo method, this method is applied to a deterministic method to investigate how accurately the perturbed eigenvalue can be estimated. The following 2-group diffusion equation is solved for the verification:

$$\begin{aligned} & D_g \nabla^2 \tilde{\phi}_g - \Sigma_{ag} \tilde{\phi}_g + \sum_{g' \neq g} \Sigma_s^{g' \to g} \tilde{\phi}_{g'} - \sum_{g' \neq g} \Sigma_s^{g \to g'} \tilde{\phi}_g \\ & + \frac{1}{\tilde{k}(a)} \sum_{g'} \left(\chi_g^p \nu_p + (1 + ai) \chi_g^d \nu_d \right) \Sigma_{fg'} \tilde{\phi}_{g'} = 0, \end{aligned} \tag{21}$$

where g =1, 2; D_g = the diffusion coefficient; Σ_{ag} = the absorption cross section; $\Sigma_s^{g' \to g}$ = the group transfer cross section from the g' th group to the gth group; and 1-group delayed neutron family is assumed. This complex-valued eigenvalue equation can easily be solved with the conventional numerical algorithm for solving an ordinary real-valued equation. It is only necessary to declare relevant variables as complex numbers in the FORTRAN statement.

A cylinder of infinite height is used for the numerical tests. The cylinder is composed of two regions. The inner region has a diameter of 40 cm, which is surrounded by an annular region with an outer diameter of 80 cm. Table 1 lists group constants that are fabricated for the numerical tests. The delayed neutron fraction $(= \nu_d / (\nu_d + \nu_p))$ is 0.002 in the inner region and 0.007 in the outer region. The

diffusion equation is solved with the finite difference method. The initial guesses of the flux are unity for the real and imaginary parts throughout the region. The initial guesses of the eigenvalue are unity and 0 for the real and imaginary parts, respectively. Fig. 1 shows the convergence criteria of the flux and eigenvalues versus the outer iteration number for a =1. The convergence criteria are defined as follows:

$$\varepsilon_{R,k} = \left| \frac{\mathrm{Re}[\tilde{k}(a)]_{n+1} - \mathrm{Re}[\tilde{k}(a)]_n}{\mathrm{Re}[\tilde{k}(a)]_n} \right|, \tag{22}$$

$$\varepsilon_{I,k} = \left| \frac{\mathrm{Im}[\tilde{k}(a)]_{n+1} - \mathrm{Im}[\tilde{k}(a)]_n}{\mathrm{Im}[\tilde{k}(a)]_n} \right|, \tag{23}$$

$$\varepsilon_{R,\phi} = \max_{i,g} \left| \frac{\mathrm{Re}[\tilde{\phi}_{g,i}]_{n+1} - \mathrm{Re}[\tilde{\phi}_{g,i}]_n}{\mathrm{Re}[\tilde{\phi}_{g,i}]_n} \right|, \tag{24}$$

$$\varepsilon_{I,\phi} = \max_{i,g} \left| \frac{\mathrm{Im}[\tilde{\phi}_{g,i}]_{n+1} - \mathrm{Im}[\tilde{\phi}_{g,i}]_n}{\mathrm{Im}[\tilde{\phi}_{g,i}]_n} \right|, \tag{25}$$

where n is the outer iteration number, and i denotes the mesh point. The outer iteration is repeated until all convergence criteria are less than 10^{-7}. Fig. 2 shows the converged flux distributions for a =1. In Fig. 2, the real parts are almost the same as the imaginary parts in both energy groups. However, the ratio of the real part to the imaginary part is arbitrary, depending on the initial guesses. The final results of the eigenvalues are completely free from the effect of the initial guesses for the eigenvalues and for the flux distributions.

The calculated real part and imaginary part of $\tilde{k}(a)$ in Eq. (21) are provided in Table 2. For comparison, an ordinary real-valued diffusion equation where ai in Eq. (21) is substituted by a is solved to obtain $k(a)$. The difference between the eigenvalue $k(a)$ and the unperturbed eigenvalue $k(0)$ is compared with $\mathrm{Im}[\tilde{k}(a)]$ in Table 2. The real part of $\tilde{k}(a)$, $\mathrm{Re}[\tilde{k}(a)]$, remains almost constant for a smaller perturbation.

The agreement between $\mathrm{Im}[\tilde{k}(a)]$ and $k(a)-k(0)$ becomes better as a becomes smaller. The effective delayed neutron fraction is calculated by the following equations:

$$\beta_{eff} \approx \frac{1}{k(0)} \frac{\mathrm{Im}[\tilde{k}(a)]}{a}, \tag{26}$$

and

$$\beta_{eff} \approx \frac{1}{\mathrm{Re}[\tilde{k}(a)]} \frac{\mathrm{Im}[\tilde{k}(a)]}{a}, \tag{27}$$

which are compared with the β_{eff} using Eq. (18) and with exact β_{eff} using Eq. (17) in Table 3. Fig. 3 shows the β_{eff} values calculated using Eqs. (18) and (27) as a function of a. The β_{eff} calculated using Eq. (18) remains almost unchanged for a larger perturbation ($a \sim 1$) compared with the exact β_{eff}. The results in Table 3 suggest that Eq. (18) could yield a relatively good approximation of the β_{eff}, even for a larger perturbation where the difference in the eigenvalue k is large enough to obtain a statistically accurate estimation of β_{eff} with a reasonable computational cost. Eq. (18) provides a good approximation for a case where the delayed and prompt sources form similar distributions. The numerical tests in Table 3 may correspond to such a situation. Eqs. (26) and (27) provide almost the same results, except for an extremely large perturbation because $\mathrm{Re}[\tilde{k}(a)]$ is extremely close to $k(0)$, except for a larger perturbation. The use of Eq. (27) is preferable to Eq. (26) because the β_{eff} can be obtained using one single calculation, which can omit the calculation of the unperturbed eigenvalue $k(0)$.

[Fig. 1], [Fig. 2], [Fig. 3], [Table 1], [Table 2], [Table 3]

2.3. Monte Carlo calculation method for solving a complex-valued equation

Next, the treatment of the complex-valued transport equation, Eq. (20), with the Monte Carlo technique is discussed. A Monte Carlo method that addresses

complex-valued neutron transport equations was developed by Yamamoto (2012) to implement the B_1 approximation method. Then, Yamamoto (2013, 2014) extended the complex-valued Monte Carlo method to reactor noise analyses to solve the frequency domain transport equation. The algorithm of the complex-valued Monte Carlo calculation can be applied to kinetics parameter calculations. In the algorithm, the complex-valued particle weight can be positive and negative. The negative weights must be cancelled by the positive weights using an appropriate weight cancellation technique. However, the cancellation of the positive and negative weights cannot occur without introducing an intentional weight cancellation technique because no two neutrons undergo collision at exactly the same point. Thus far, certain techniques have been proposed for this weight cancellation (Booth and Gubernatis, 2010; Yamamoto, 2011; Bo and Petrovic, 2012). This paper uses the "binning procedure" for the weight cancellation (Yamamoto, 2009; Yamamoto, 2011). The entire region where fission can occur is divided into many small regions (bins). Fission sources with positive and negative weights accumulate in the bins. If the size of each bin is small enough, then the bias caused by the binning procedure can be negligibly small. The positive and negative weights in each bin are summed (cancelled) at the end of each cycle.

The calculation flow for the β_{eff} is shown below:

(1) The entire region where fission can occur is divided into small bins.

(2) At the beginning of each cycle, particles are started from the fission source sites determined from the fission source distribution inherited from the previous cycle. In the first cycle, a user-specified initial source distribution, which can be real or complex numbers, is used. The particle weights are always complex numbers after the second cycle even when a real-valued initial source distribution is used in the first cycle. The energy of the starter particle is determined as follows: First, whether

the starting neutron is delayed or prompt is decided. If

$$\xi < \beta \frac{1+a}{1+a\beta}, \tag{28}$$

then the neutron is a delayed neutron, otherwise, the neutron is a prompt neutron, where ξ is a uniform pseudo random number from [0, 1], and $\beta = \nu_d /(\nu_d + \nu_p)$. The energy is determined from χ^d or χ^p, depending on whether the neutron is a delayed or prompt neutron, respectively. The weight of the *n*th starting particle in the *k*th bin is $\tilde{W}_s^n = \tilde{W}_{s,k}$ for a prompt neutron and is $\tilde{W}_s^n = \tilde{W}_{s,k}(1+ai)/(1+a)$ for a delayed neutron, where $\tilde{W}_{s,k}$ is a complex-valued starting weight in the *k*th bin. $\tilde{W}_{s,k}$ is defined later.

(3) The particles are tracked in the same manner as conventional real-valued transport problems.

(4) At each collision site, the number of sources used for the next cycle is estimated as follows:

$$\tilde{S}_{k,\ell} = (\nu_p + \nu_d)\frac{\Sigma_{f,k}}{\Sigma_{t,k}}\tilde{W}_\ell, \tag{29}$$

where the index *k* stands for a bin number, ℓ is summed over all collisions in a cycle, and $\tilde{W}_\ell$ is a complex-valued particle weight before the ℓth collision. As stated above, the tilde denotes a complex number. $\tilde{S}_{k,\ell}$ can also be obtained by the track length estimator as follows:

$$\tilde{S}_{k,\ell} = (\nu_p + \nu_d)\Sigma_{f,k} t_{k,\ell}\tilde{W}_\ell, \tag{30}$$

where $t_{k,\ell}$ is a track length in the *k*th bin and in the ℓth trajectory.

(5) At each collision site, both the real and imaginary parts of the complex-valued weight are reduced from the probability of absorption as follows:

$$\tilde{W}'_\ell = \tilde{W}_\ell \frac{\Sigma_s}{\Sigma_t} = \mathrm{Re}[\tilde{W}_\ell]\frac{\Sigma_s}{\Sigma_t} + i\cdot \mathrm{Im}[\tilde{W}_\ell]\frac{\Sigma_s}{\Sigma_t}, \tag{31}$$

where $\tilde{W}'_\ell$ = the weight after the weight reduction at the ℓ th collision site.

(6) The Russian roulette game is separately applied to the real and imaginary parts when either or both $|\mathrm{Re}[W'_\ell]|$ and $|\mathrm{Im}[W'_\ell]|$ are less than a prescribed lower weight boundary. When either the real or imaginary part is killed but the other part still survives, then the weight is continually transported until both parts are simultaneously killed. The weight of an imaginary part is generally much smaller than that of a real part. The lower weight boundary of the imaginary part should be smaller than that of the real part. As the perturbation parameter *a* becomes smaller, $|\mathrm{Im}[W_\ell]|$ becomes smaller as well. Thus, the lower weight boundary for the imaginary part must be adjusted depending on the parameter *a*.

(7) After all of the random walk processes within one cycle are completed, the complex-valued eigenvalue is estimated as follows:

$$\tilde{k}(a) = \frac{\sum_\ell (\nu_p + (1+ai)\nu_d)\frac{\Sigma_f}{\Sigma_t}\tilde{W}_\ell}{\sum_n \tilde{W}_s^n}, \tag{32}$$

where ℓ is summed over all collisions in the current cycle, and *n* is summed over all starter fission sources of the current cycle inherited from the previous cycle. The denominator is a sum of the weights of all starting particles in the cycle. Again, $\tilde{k}(a)$ can be obtained using the track length estimator.

(8) The fission sources used for the next cycle are obtained as follows: The number of starting particles in the *k*th bin for the next cycle is determined using the following equation:

$$n_k = Int\left(\max\left(\left|\mathrm{Re}\left[\tilde{S}_k\right]\right|, \left|\mathrm{Im}\left[\tilde{S}_k\right]\right|, 1\right) + \xi\right), \tag{33}$$

where Int(·)= the integer part, $\tilde{S}_k = \sum_\ell \tilde{S}_{k,\ell}$, and ℓ is summed over all collisions in the *k*th bin within the cycle. $\tilde{W}_{s,k}$ used in the step (2) is provided by the following equation:

$$\tilde{W}_{s,k} = \frac{\tilde{S}_k}{n_k} \cdot \frac{N}{M}, \tag{34}$$

where *N* is the nominal number of source particles per cycle, and $M = \sum_k n_k$. Although the total number of starting particles for the next cycle is *M* rather than *N*, the weight is normalized as if *N* particles started in each cycle. The starting particles are uniformly distributed within the bin.

2.4. Numerical examples of β_{eff} calculations with the *Monte Carlo* method

Using the new Monte Carlo calculation method explained above, β_{eff} calculations were performed for cylindrical geometries of infinite height. This new method has not yet been implemented into a production Monte Carlo code. A simple test program has been developed to perform the numerical tests. For the numerical examples, 3 energy group constants were prepared with the standard reactor analysis code SRAC (Okumura et al., 2007). The first example is composed of a low-enriched light-water moderated UO_2 fuel rod array surrounded by a light-water reflector. The outer diameter of the fuel rod is 1.25 cm. The square lattice pitch is 1.956 cm, which corresponds to a water-to-fuel volume ratio of 1.83. The region of the fuel rod array has a diameter of 24.4 cm, and the thickness of the light-water reflector is 30 cm. The 3 group constants of the homogenized UO_2 fuel rod array and of the light-water reflector are provided in Table 4. The scattering was assumed isotropic, and up-scattering was neglected.

The eigenvalue calculations with a complex-valued perturbation were performed with 50,000 neutrons per cycle, skipping 20 cycles and running 2,000 active cycles. The

unperturbed and perturbed eigenvalues, $k(0)$ and $k(a)$, were calculated with 50,000 neutrons per cycle, skipping 20 cycles and running 10,000 active cycles. As stated in Sec. 2.2, the imaginary part in the initial source distribution can be arbitrary. In this paper, the imaginary part is tentatively set to 0 to see how the real-valued initial source distribution works. The lower weight boundaries for the Russian roulette game were 0.001 and 0.0001 for the real part and for the imaginary part, respectively. The homogenized fuel region was divided into 854 concentric rings where the positive and negative weights were cancelled. As a reference for comparison with a deterministic method, the discrete ordinates transport calculation code DANTSYS (Alcouffe et al., 1995) was used to calculate the exact β_{eff} defined by Eq. (17), with the same group constants. The accuracy of this new method has already been demonstrated by the deterministic diffusion calculations in Sec. 2.2. The purpose of the numerical examples focuses on how efficiently the new method calculates the β_{eff} compared with two independent Monte Carlo calculations. The calculated results are provided in Table 5 for a = 0.1, 0.5, 1.0, 1.5, and 3.0. The relative figure of merit, which is defined by 1/(cpu time)/(square of one fractional standard deviation), is provided for each β_{eff}. The newly developed method (Eq. (27)) can provide an extremely good estimate of the β_{eff} compared with the exact β_{eff} calculated using the deterministic method. Furthermore, the newly developed method outperforms the method using Eq. (18) in terms of the computational efficiency. In this numerical example, the linearity between a and $k(a)-k(0)$ is kept for a larger a. Thus, a relatively good β_{eff} can be obtained by Eq. (18). However, if the linearity were kept only for a smaller perturbation, then Eq. (18) could no longer be available. In contrast, the newly developed method can provide an accurate β_{eff} with a small statistical uncertainty for a small perturbation.

[Table 4], [Table 5]

The next example addresses a fast system where a metal plutonium (^{239}Pu:^{240}Pu= 95.3 wt%:4.7 wt%) cylinder is surrounded by a graphite reflector. The region of the metal fuel has a diameter of 4.12 cm, and the thickness of the graphite reflector is 20 cm. The fuel region was divided into 268 concentric rings for the weight cancellation. The 3-group constants for this example are provided in Table 4. The calculations were performed in the same manner as in the previous example. The results are shown in Table 6 for a = 0.1, 0.5, 1.0, 3.0, and 10.0. Although the β_{eff} of a plutonium system is much smaller than that of a uranium system, this value can be accurately estimated using the newly developed method with a small statistically uncertainty.

[Table 6]

3. Monte Carlo Calculation of Λ

3.1. Theory of complex-valued perturbation method

Verboomen et al. (2006) proposed a method for calculating a prompt neutron generation time Λ without an explicit solution for the adjoint flux. In this method, a fictitious 1/v-absorber is uniformly introduced in the system. The transport eigenvalue equation with an introduced 1/v-absorber is as follows:

$$\mathbf{H}\phi(\mathbf{r},\mathbf{\Omega},E;c)+\frac{c}{\upsilon(E)}\phi(\mathbf{r},\mathbf{\Omega},E;c)=\frac{1}{k(c)}S_f(\mathbf{r},\mathbf{\Omega},E;c)\,, \tag{35}$$

where $\upsilon(E)=$ the velocity of a neutron with energy E, and c = the parameter for perturbation,

$$S_f(\mathbf{r},\mathbf{\Omega},E;c)=S_f^p(\mathbf{r},\mathbf{\Omega},E;c)+\sum_j S_{f,j}^d(\mathbf{r},\mathbf{\Omega},E;c), \tag{36}$$

$$S_f^p(\mathbf{r},\mathbf{\Omega},E;c)=\sum_m\frac{\chi_m^p(E)}{4\pi}\int_{4\pi}d\mathbf{\Omega}'\int dE'\nu_m^p(E')\Sigma_{f,m}(\mathbf{r},E')\phi(\mathbf{r},\mathbf{\Omega}',E';c), \tag{37}$$

$$S^d_{f,j}(\mathbf{r},\mathbf{\Omega},E;c)=\sum_m \frac{\chi^d_{m,j}(E)}{4\pi}\int_{4\pi} d\mathbf{\Omega}'\int dE'\nu^d_{m,j}(E')\Sigma_{f,m}(\mathbf{r},E')\phi(\mathbf{r},\mathbf{\Omega}',E';c)\,. \quad (38)$$

We take the inner product of Eq. (35) with the adjoint flux in the unperturbed system (i.e., the solution of Eq. (11)). Then, we take the inner product of Eq. (11) with $\phi(\mathbf{r},\mathbf{\Omega},E;c)$ of Eq. (35), and subtract one inner product from the other. As a result, we obtain the following equation:

$$\frac{1}{c}\left(\frac{1}{k(c)}-\frac{1}{k(0)}\right)=\frac{\left\langle \phi^*(\mathbf{r},\mathbf{\Omega},E)\frac{1}{\upsilon(E)}\phi(\mathbf{r},\mathbf{\Omega},E;c)\right\rangle}{\left\langle \phi^*(\mathbf{r},\mathbf{\Omega},E)S_f(\mathbf{r},\mathbf{\Omega},E;c)\right\rangle}\,. \quad (39)$$

The limit of Eq. (39) as c approaches zero becomes the following equation:

$$\lim_{c\to 0}\frac{1}{c}\left(\frac{1}{k(c)}-\frac{1}{k(0)}\right)=\Lambda=\frac{\left\langle \phi^*(\mathbf{r},\mathbf{\Omega},E)\frac{1}{\upsilon(E)}\phi(\mathbf{r},\mathbf{\Omega},E)\right\rangle}{\left\langle \phi^*(\mathbf{r},\mathbf{\Omega},E)S_f(\mathbf{r},\mathbf{\Omega},E)\right\rangle}\,. \quad (40)$$

If the parameter c is small enough, then an approximate Λ value can be obtained using the following equation:

$$\Lambda\approx\frac{1}{c}\left(\frac{1}{k(c)}-\frac{1}{k(0)}\right). \quad (41)$$

This method can be easily implemented into Monte Carlo calculation codes, with minor modifications. However, if the linearity between c and $1/k(c)-1/k(0)$ (= reactivity due to adding the 1/v-absorber) does not hold for a larger c, then the small reactivity must be calculated with a high accuracy by spending much computational resources.

Next, the newly developed method for β_{eff} calculations is applied to Λ calculations. For Λ calculations, the following complex-valued transport equation is solved:

$$\mathbf{H}\tilde{\phi}(\mathbf{r},\mathbf{\Omega},E;c)+\frac{ic}{\upsilon(E)}\tilde{\phi}(\mathbf{r},\mathbf{\Omega},E;c)=\frac{1}{\tilde{k}(c)}\tilde{S}_f(\mathbf{r},\mathbf{\Omega},E;c)\,, \quad (42)$$

where the tilde denotes a complex-valued quantity. The Monte Carlo algorithm for solving Eq. (42) is almost identical to that for β_{eff}. Thus, the Monte Carlo algorithm for Λ calculations can be realized by setting a = 0 in the calculation flow in Sec.2.3. However, the second term on the left-hand side of Eq. (42) must be considered in the random walk process of the Monte Carlo calculation for Λ. This technique has already been established for B_1 approximation calculations and for frequency domain calculations (Yamamoto, 2012; Yamamoto, 2013; Yamamoto, 2014). Due to the second term on the left-hand side of Eq. (42), the particle weight continuously changes as the particle flies. The weight change rate of a particle that flies an infinitesimal distance *ds* is described by the following equation:

$$\frac{d\tilde{W}}{\tilde{W}} = -\frac{ic}{\upsilon(E)} ds \ . \tag{43}$$

After the particle flies a distance s_ℓ in the ℓ th flight path, the initial weight $\tilde{W}_\ell$ changes to the following equation:

$$\tilde{W}_{\ell+1} = \tilde{W}_\ell \exp\left(-\frac{ic}{\upsilon_\ell(E)} s_\ell \right). \tag{44}$$

Because the complex-valued weight continuously changes as the particle moves, the product of the track length and weight is provided by the following equation:

$$\tilde{T}_\ell = \int_0^{s_\ell} \tilde{W}_\ell \exp\left(-\frac{ic}{\upsilon_\ell(E)} s'_\ell \right) ds'_\ell = \tilde{W}_\ell \frac{i\upsilon_\ell(E)}{c} \left(\exp\left(-\frac{ic}{\upsilon_\ell(E)} s_\ell \right) - 1 \right). \tag{45}$$

Thus, $t_{k,\ell}\tilde{W}_\ell$ in Eq. (30) is replaced by $\tilde{T}_\ell$ of Eq. (45). The free flight distance is sampled as usual by $-\ell n\xi / \Sigma_t$, where ξ is a uniform pseudo random number from [0, 1]. The effect of $c/\upsilon(E)$ is already included in Eq. (44). Thus, $c/\upsilon(E)$ is not used for sampling the next collision points (Yamamoto, 2012).

3.2. Verification using a deterministic method

For verification of the newly developed method for Λ calculations, the following 2-group complex-valued diffusion equation was solved:

$$\begin{aligned} & D_g \nabla^2 \tilde{\phi}_g - \Sigma_{ag} \tilde{\phi}_g + \sum_{g' \neq g} \Sigma_s^{g' \to g} \tilde{\phi}_{g'} - \sum_{g' \neq g} \Sigma_s^{g \to g'} \tilde{\phi}_g \\ & - \frac{ic}{\upsilon_g} \tilde{\phi}_g + \frac{1}{\tilde{k}(c)} \sum_{g'} \left(\chi_g^p \nu_p + \chi_g^d \nu_d \right) \Sigma_{fg'} \tilde{\phi}_{g'} = 0. \end{aligned} \tag{46}$$

where g =1, 2. Numerical tests were performed for a cylindrical fuel with a diameter of 65 cm, which was surrounded by an annular reflector with an outer diameter of 130 cm. The 2 group constants used for the calculations are provided in Table 7. The calculated real and imaginary parts of $\tilde{k}(c)$ of Eq. (46) are provided in Table 8. The prompt neutron generation time Λ was estimated using three methods. One method is an exact Λ calculated by the perturbation theory as defined in Eq. (40). The second method uses Eq. (41) where an approximate Λ is calculated using the change in eigenvalues. The third method is provided by the following equation:

$$\Lambda \approx \frac{1}{c} \left(\frac{1}{\mathrm{Re}[\tilde{k}(c)]} - \frac{1}{\mathrm{Re}[\tilde{k}(c)] + \Delta k} \right), \tag{47}$$

where

$$\Delta k = \frac{\mathrm{Im}[\tilde{k}(c)](\mathrm{Re}[\tilde{k}(c)]^2 + \mathrm{Im}[\tilde{k}(c)]^2)}{\mathrm{Re}[\tilde{k}(c)](\mathrm{Re}[\tilde{k}(c)] - \mathrm{Im}[\tilde{k}(c)])}. \tag{48}$$

The formulation of Eqs. (47) and (48) is found through trial and error such that the Λ is as close as possible to the exact value. Refer to the Appendix for the derivation of Eq. (48). This formulation yields an almost constant and exact Λ, regardless of parameter c, as shown in Table 8. In contrast, the approximate Λ obtained by Eq. (41) deviates from the exact value as the perturbation becomes larger.

[Table 7], [Table 8]

3.3. Numerical examples of Λ calculations using the *Monte Carlo* method

The two test problems for the β_{eff} in Sec. 2.4 were used again for the numerical tests of Λ calculations with the newly developed Monte Carlo method. The calculational conditions of the Monte Carlo calculations were identical to those conditions in Sec. 2.4. The calculated results of the Λ for the UO_2 fuel rod array for c = 20, 40, 80, 100, and 200 are provided in Table 9. For the plutonium metal, the results for c = 300, 500, 1000, 2000, and 4000 are provided in Table 10. For comparison, DANTSYS code (Alcouffe et al., 1995) was used for calculating the exact Λ by Eq. (40) with the same group constants. For both the thermal and fast systems, the Λ values calculated using the newly developed method agree well with the exact one calculated using the deterministic method. The newly developed method outperforms the method using Eq. (41) in terms of the computational efficiency.

[Table 9], [Table 10]

4. Conclusions

This paper proposes a new method in which a complex-valued quantity is added to the transport eigenvalue equation as a perturbation for the kinetics parameter calculation. For the β_{eff} calculation, this paper adopts a perturbation method proposed by Nagaya and Mori (2011). An exact β_{eff} can be obtained by taking the infinitesimally small limit of the perturbation. An accurate approximation to the exact β_{eff} can be obtained for a small perturbation. However, the previously proposed Monte Carlo method requires a large computational cost for an accurate estimation of the approximate β_{eff} because the difference in two eigenvalues calculated by two independent Monte Carlo runs must be obtained with a small statistical uncertainty. The new method proposed in this paper can provide the perturbed and unperturbed eigenvalues using one single Monte Carlo run, thereby achieving high computational efficiency.

For the Λ calculation, this paper adopts a perturbation method proposed by Verboomen et al. (2006) in which a 1/*v*-absorber is homogenously added in an unperturbed system. Again, the newly proposed method in this paper can provide an extremely accurate Λ with much less computational cost.

The proposed method is based on a conjecture that the real part and imaginary part of the eigenvalue of a complex-valued eigenvalue equation are close approximations to the unperturbed eigenvalue and to the change in the eigenvalue due to the perturbation, respectively. The mathematical verification of the conjecture has not been presented in this paper. The proof will be one of our future works to strengthen the basis of the proposed method. Some numerical examples are presented to corroborate this conjecture.

A technique that uses complex-valued weights has already been implemented into the MCNP code (Briesmeister, 2000) by Yamamoto (2012). Thus, the development of a viable method for weight cancellation or a novel method for avoiding weight cancellation must be performed to bring the new method into a production Monte Carlo code.

Appendix

The derivation of Eq. (48) is presented in this Appendix. The inverse of $\tilde{k}(c)$ is defined as follows:

$$\tilde{\lambda} \equiv \frac{1}{\tilde{k}(c)} = \mathrm{Re}[\tilde{\lambda}] + i \cdot \mathrm{Im}[\tilde{\lambda}], \tag{A1}$$

where

$$\mathrm{Re}[\tilde{\lambda}] = \frac{\mathrm{Re}[\tilde{k}(c)]}{\mathrm{Re}[\tilde{k}(c)]^2 + \mathrm{Im}[\tilde{k}(c)]^2}, \tag{A2}$$

$$\mathrm{Im}[\tilde{\lambda}] = -\frac{\mathrm{Im}[\tilde{k}(c)]}{\mathrm{Re}[\tilde{k}(c)]^2 + \mathrm{Im}[\tilde{k}(c)]^2}. \quad \text{(A3)}$$

We assume that the unperturbed and perturbed k_{eff} values are approximated as $1/\mathrm{Re}[\tilde{\lambda}]$ and $1/(\mathrm{Re}[\tilde{\lambda}]+\mathrm{Im}[\tilde{\lambda}])$, respectively. As a result, we obtain Δk, which is the difference of k_{eff} due to the addition of $1/v$ absorber, as follows:

$$\Delta k = \frac{1}{\mathrm{Re}[\tilde{\lambda}]+\mathrm{Im}[\tilde{\lambda}]} - \frac{1}{\mathrm{Re}[\tilde{\lambda}]}$$

$$= \frac{\mathrm{Im}[\tilde{k}(c)](\mathrm{Re}[\tilde{k}(c)]^2+\mathrm{Im}[\tilde{k}(c)]^2)}{\mathrm{Re}[\tilde{k}(c)](\mathrm{Re}[\tilde{k}(c)]-\mathrm{Im}[\tilde{k}(c)])}. \quad \text{(A4)}$$

References

Alcouffe, R.E., Baker, R.S., Brinkley, F.W., Marr, D.R., O'Dell, R.D., Walters, W.F., 1995. DANTSYS: A diffusion accelerated neutral particle transport code system, LA-12969-M.

Bécares, V., Pérez-Martín, S., Vázquez-Antolín, M., Villamarín D., Martín-Fuertes, F., González-Romero, E.M., Merino, I., 2014. Review and comparison of effective delayed neutron fraction calculation methods with Monte Carlo codes. Ann. Nucl. Energy, 65, 402-410.

Booth, T.E., Gubernatis, J.E., 2010. Exact regional Monte Carlo weight cancellation for second eigenfunction calculations. Nucl. Sci. Eng., 165, 283–291.

Bretscher, M.M, 1997. Perturbation-independent methods for calculating research reactor kinetic parameters. ANL/RERTR/TM-30.

Briesmeister, J.F., Ed., 2000. MCNP—A general Monte Carlo N-particle transport code, version 4C. LA-13709-M.

Carta, M., Dulla, S., Peluso, V., Ravetto, P., Bianchini, G., 2011. Calculation of the

effective delayed neutron fraction by deterministic and Monte Carlo methods. Sci. Technol. Nucl. Installations, Article ID 584256.

Feghhi, S., Shahriari, M., Afarideh, H., 2008. Calculation of the importance-weighted neutron generation time using MCNIC method. Ann. Nucl. Energy, 35, 1397–1402.

Kiedrowski, B.C., Brown, F.B., Wilson, P.P., 2011. Adjoint-weighted tallies for k-eigenvalue calculations with continuous-energy Monte Carlo. Nucl. Sci. Eng., 168, 226–241.

Leppänen, J., Aufiero, M., Fridman, E., Rachamin, R., van der Marck, S., 2014. Calculation of effective point kinetics parameters in the Serpent 2 Monte Carlo code. Ann. Nucl. Energy, 65, 272–279.

Meulekamp, R.K., van der Marck, S.C., 2006. Calculating the effective delayed neutron fraction with Monte Carlo. Nucl. Sci. Eng., 152, 142–148.

Nagaya, Y., Chiba, G., Mori, T., Irwanto, D., Nakajima, K., 2010. Comparison of Monte Carlo calculation methods for effective delayed neutron fraction, Ann. Nucl. Energy, 37, 1308-1315.

Nagaya, Y., Mori, T., 2011. Calculation of effective delayed neutron fraction with Monte Carlo perturbation techniques. Ann. Nucl. Energy, 38, 254–260.

Nauchi, Y., Kameyama, T., 2005. Proposal of direct calculation of kinetic parameters β_{eff} and Λ based on continuous energy Monte Carlo method. J. Nucl. Sci. Technol., 42, 503–514.

Nauchi, Y., Kameyama, T., 2010. Development of calculation technique for Iterated Fission Probability and reactor kinetic parameters using continuous-energy Monte Carlo method. J. Nucl. Sci. Technol., 47, 977–990.

Okumura, K., Kugo, T., Kaneno, K., Tsuchihashi, K., 2007. SRAC2006: A comprehensive neutronics calculation code system. JAEA-Data/Code 2007-004.

Raskach, K.F., Blyskavka, A.A., 2010. An experience of applying iterated fission probability method to calculation of effective kinetics parameters and keff sensitivities with Monte Carlo. In: Proc. of PHYSOR 2010 –Advances in Reactor Physics to Power the Nuclear Renaissance, Pittsburgh, PA, USA, May 9–14, 2010. American Nuclear Society, LaGrange Park, IL.

Shi, B., Petrovic, B., 2012. Calculating the second eigenpair in criticality calculations using the Monte Carlo method with source points pairing as an efficient net-weight (cancellation) algorithm. Nucl. Sci. Eng., 172, 138–150.

Shim, H.J., Kim, C.H., Kim, Y., 2010. Estimation of adjoint-weighted kinetics parameters in Monte Carlo forward calculations. In: Proc. of PHYSOR 2010 –Advances in Reactor Physics to Power the Nuclear Renaissance, Pittsburgh, PA, USA, May 9–14, 2010. American Nuclear Society, LaGrange Park, IL.

Verboomen, B., Haeck, W., Baeten, P., 2006. Monte Carlo calculation of the effective neutron generation time. Ann. Nucl. Energy, 33, 911–916.

Yamamoto, T., 2009. Convergence of the second eigenfunction in Monte Carlo power iteration. Ann. Nucl. Energy, 36, 7–14.

Yamamoto, T., 2011. Non-regionwise weight cancellation for Monte Carlo higher order criticality calculations using kernel density estimator. Ann. Nucl. Energy, 38, 2515–2520.

Yamamoto, T., 2012. Monte Carlo method with complex weights for neutron leakage-corrected calculations and anisotropic diffusion coefficient generations. Ann. Nucl. Energy, 50, 141–149.

Yamamoto, T., 2013. Monte Carlo method with complex-valued weights for frequency domain analyses of neutron noise, Ann. Nucl. Energy, 58, 72–79.

Yamamoto, T., 2014. Frequency domain Monte Carlo simulation method for cross

power spectral density driven by periodically pulsed spallation neutron source using complex-valued weight Monte Carlo method. Ann. Nucl. Energy, 63, 711–720.

Figure legends

Fig. 1 Convergence criteria for eigenvalue and flux versus outer iteration number for $a = 1$.

Fig. 2 Converged flux distributions by the complex-valued diffusion calculation for $a = 1$.

Fig. 3 β_{eff} by Eqs. (18) and (27) as a function of a.

Figure1

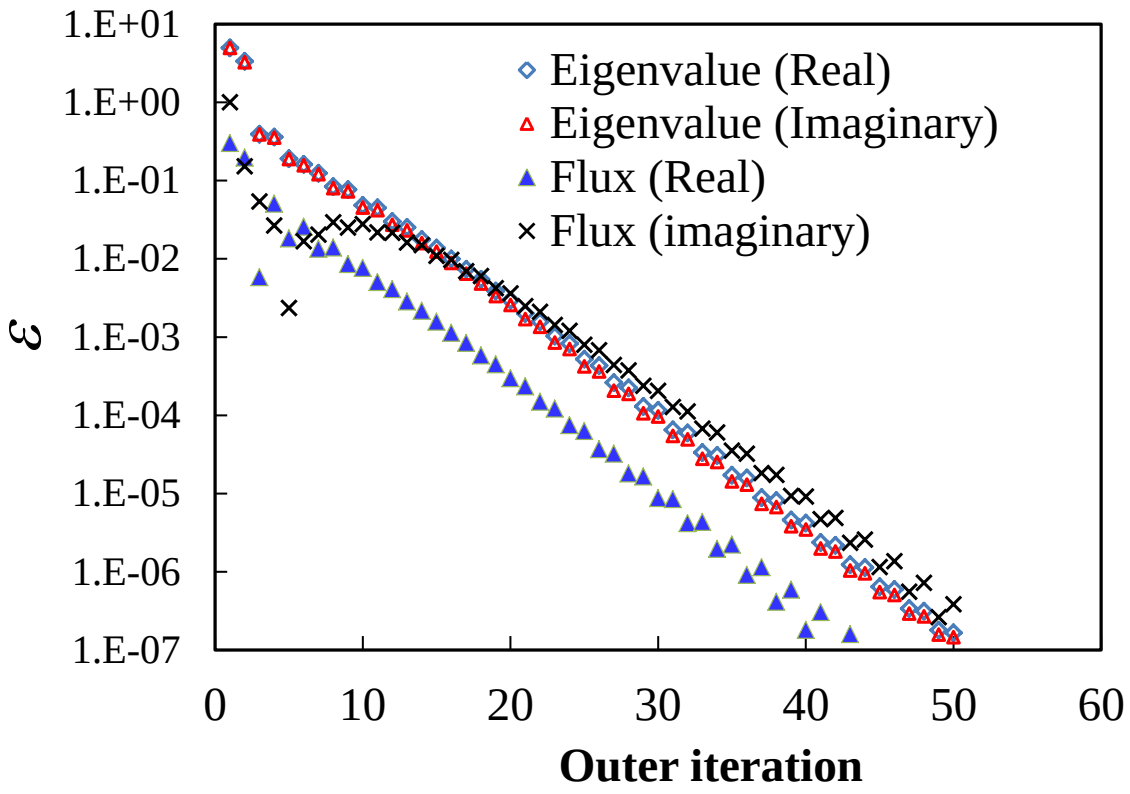

Fig. 1 Convergence criteria for eigenvalue and flux versus outer iteration number for $a = 1$.

Figure2

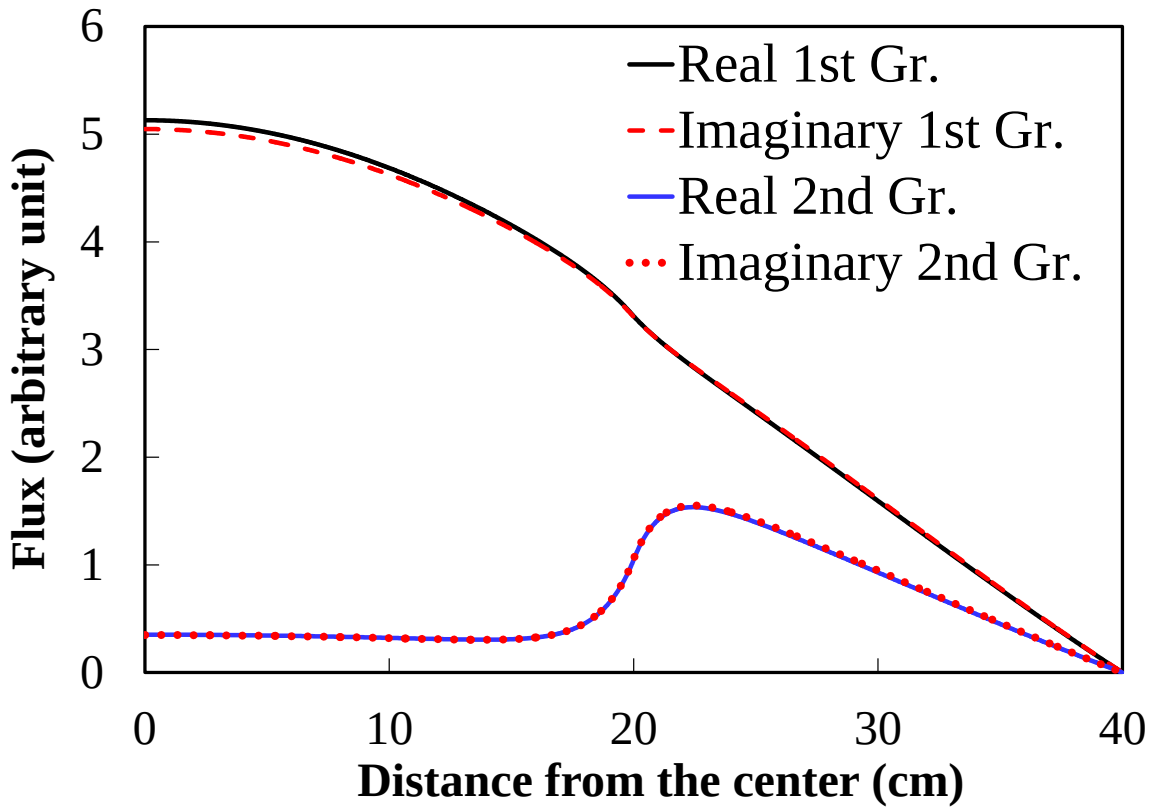

Fig. 2 Converged flux distributions by the complex-valued diffusion calculation for a = 1.

Figure3

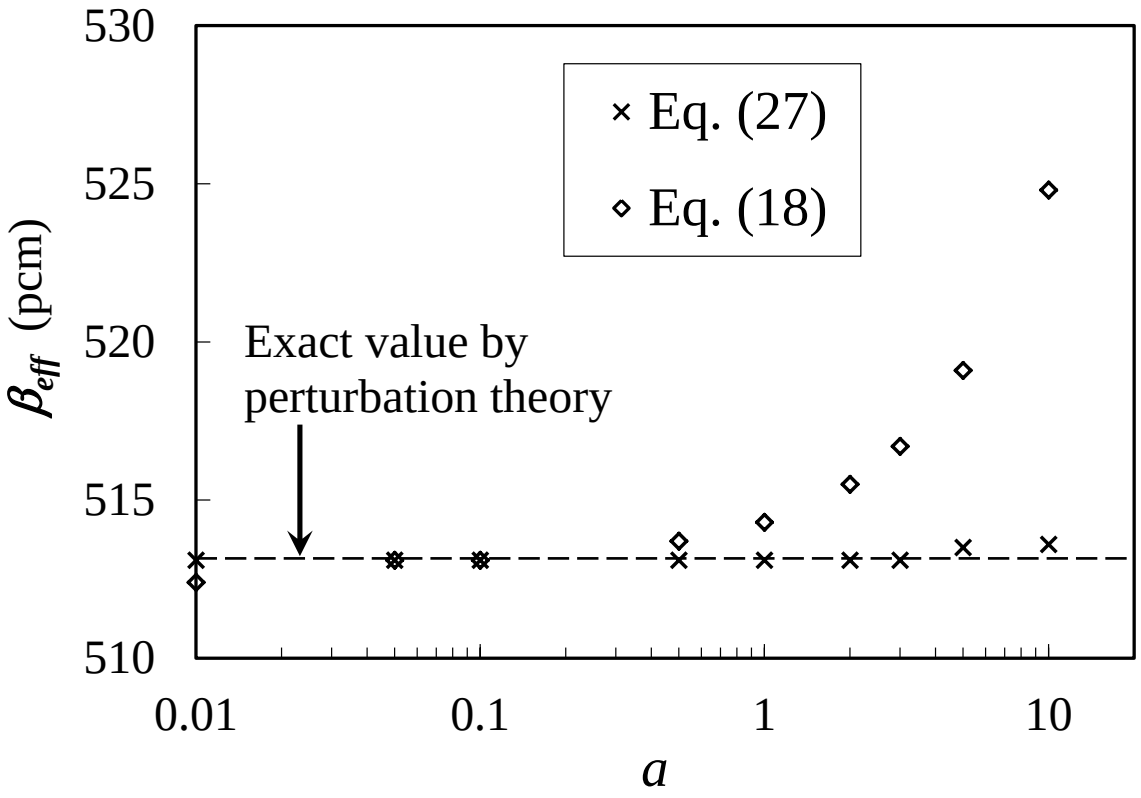

Fig. 3 β_{eff} by Eqs. (18) and (27) as a function of a.

Table1

Table 1 2-group constants for β_{eff} calculation.

	Inner region	Outer region
D_1(cm)	1.111	1.190
D_2(cm)	0.1667	0.1587
Σ_{f1} (cm^{-1})	0.005	0.001
Σ_{f2} (cm^{-1})	0.04	0.036
Σ_{a1} (cm^{-1})	0.013	0.005
Σ_{a2} (cm^{-1})	0.09	0.096
$\Sigma_s^{1\to2}$ (cm^{-1})	0.00574	0.055
$\Sigma_s^{2\to1}$ (cm^{-1})	0	0
ν_p	2.994	2.979
ν_d	0.006	0.021
$\nu_p/(\nu_p+\nu_d)$	0.002	0.007
χ_1^p	0.98	0.98
χ_2^p	0.02	0.02
χ_1^d	0.5	0.5
χ_2^d	0.5	0.5

Table2

Table 2 Real part and imaginary part of eigenvalues of the diffusion equation, Eq. (21), and comparison with the direct eigenvalue calculations.

a	$\mathrm{Re}[\tilde{k}(a)]$	$\mathrm{Im}[\tilde{k}(a)]$	$k(a)-k(0)$
0	1.00686	0	0
0.01	1.00686	5.1658E-5[a]	5.1600E-5
0.05	1.00686	2.5829E-4	2.5830E-4
0.1	1.00682	5.1658E-4	5.1670E-4
0.5	1.00682	2.5829E-3	2.5859E-3
1	1.00685	5.1658E-3	5.1780E-3
2	1.00681	1.0332E-2	1.0380E-2
3	1.00675	1.5499E-2	1.5607E-2
5	1.00656	2.5849E-2	2.6132E-2
10	1.00563	5.1707E-2	5.2843E-2
50	0.97486	2.6599E-1	2.8271E-1

[a] Read as 5.1658×10^{-5}

Table3

Table 3 Comparison of β_{eff} (pcm) by Eqs. (26), (27), and (18) with the exact one.

a	Exact (Eq. (17))	Eq. (26)	Eq. (27)	Eq. (18)
−1		513.1	513.1	511.8*
0.01		513.1	513.1	512.4
0.05		513.1	513.1	513.1
0.1		513.1	513.1	513.1
0.5		513.1	513.1	513.7
1	513.1	513.1	513.1	514.3
2		513.1	513.1	515.5
3		513.1	513.2	516.7
5		513.5	513.6	519.1
10		513.6	514.2	524.8
50		528.4	545.7	561.6

*prompt method

Table4

Table 4 3-group constants for UO_2 fuel rod array, light-water reflector, Pu metal, and graphite reflector

	UO_2 fuel rod array	Light-water reflector	Pu metal	Graphite reflector
Σ_{t1} (cm^{-1})	0.29829	0.33207	0.28573	0.21053
Σ_{t2} (cm^{-1})	0.83334	1.1265	0.35423	0.45009
Σ_{t3} (cm^{-1})	1.6389	2.7812	0.62448	0.53500
Σ_{f1} (cm^{-1})	0.0030586	—	0.072424	—
Σ_{f2} (cm^{-1})	0.0021579	—	0.052973	—
Σ_{f3} (cm^{-1})	0.056928	—	0.13267	—
Σ_{a1} (cm^{-1})	0.003385	0.00030500	0.073056	0.00013890
Σ_{a2} (cm^{-1})	0.11895	0.00036990	0.064640	0.0000017
Σ_{a3} (cm^{-1})	0.086180	0.018250	0.022681	0.000021
$\Sigma_s^{1\to2}$ (cm^{-1})	0.073843	0.10464	0.029374	0.029672
$\Sigma_s^{2\to3}$ (cm^{-1})	0.043803	0.097961	0.00030767	0.015913
ν_p	2.3831	—	3.1934	—
ν_d	0.016905	—	0.00662	—
χ_1^p	0.88149	—	0.77541	—
χ_2^p	0.11851	—	0.22362	—
χ_3^p	0	—	0.00097120	—
χ_1^d	0.41461	—	0.16598	—
χ_2^d	0.58539	—	0.81806	—
χ_3^d	0	—	0.015953	—
υ_1(cm/s)	1.6674×10^9	1.6674×10^9	1.9128×10^9	1.9128×10^9
υ_2(cm/s)	1.7373×10^7	1.7373×10^7	6.9765×10^8	6.9765×10^8
υ_3(cm/s)	3.4685×10^5	3.4685×10^5	1.6899×10^7	1.6899×10^7

Table5

Table 5 Comparison of β_{eff} (pcm) by Eq. (27) and Eq. (18) with the exact one (UO_2 fuel rod array)

a	Re$[\tilde{k}(a)]$	Im$[\tilde{k}(a)]$	β_{eff} (pcm) by Eq. (27)	$k(a)-k(0)$ [c]	β_{eff} (pcm) by Eq. (18)	β_{eff} (pcm) by DANTSYS
0.1	1.001556 ±0.000057	7.564E-4[a] ±1.5E-6[b]	755.3 ±1.5 (157)[d]	—	—	756.7
0.5	1.001534 ±0.000058	3.7893E-3 ±3.4E-6	756.7 ±0.7 (729)	0.003726 ±3.6E-5	744.1 ±7.1 (1)	
1.0	1.001517 ±0.000057	7.5785E-3 ±4.8E-6	756.7 ±0.5 (1461)	0.007556 ±3.6E-5	755.4 ±3.6 (4)	
1.5	1.001604 ±0.000058	1.1363E-2 ±6E-6	756.3 ±0.4 (2297)	0.011417 ±3.6E-5	756.0 ±2.3 (9)	
3.0	1.001528 ±0.000058	2.2721E-2 ±8E-6	756.2 ±0.3 (4534)	0.027400 ±3.6E-5	756.0 ±1.2 (36)	
-1.0[e]	—	—	—	-0.007592 ±3.5E-5	758.0 ±3.5 (4)	

[a] Read as 7.564×10^{-4}.

[b] one standard deviation

[c] $k(0)=1.001537\pm0.000025$

[d] Relative figure of merit with respect to "β_{eff} by Eq. (18) and a = 0.5"

[e] "prompt method"

Table6

Table 6 Comparison of β_{eff} (pcm) by Eq. (27) and Eq. (18) with the exact one (Pu metal)

a	Re[$\tilde{k}(a)$]	Im[$\tilde{k}(a)$]	β_{eff} (pcm) by Eq. (27)	$k(a)-k(0)$ [c]	β_{eff} (pcm) by Eq. (18)	β_{eff} (pcm) by DANTSYS
0.1	0.999597 ±0.000065	2.121E-4[a] ±9E-7[b]	212.1 ±0.9 (8.9E+2)[d]	—	—	212.6
0.5	0.999524 ±0.000065	1.0620E-3 ±2.0E-6	212.5 ±0.4 (4.3E+3)	0.001069 ±4.0E-5	213.8 ±8.0 (1)	
1.0	0.999466 ±0.000064	2.1239E-3 ±2.9E-6	212.5 ±0.3 (9.1E+3)	0.002135 ±4.7E-5	213.6 ±4.7 (3)	
3.0	0.999519 ±0.000063	6.3803E-3 ±5.1E-6	212.8 ±0.2 (2.7E+4)	0.006383 ±4.0E-5	212.9 ±1.3 (18)	
10.0	0.999438 ±0.000065	2.1238E-2 ±9E-6	212.5 ±0.1 (7.1E+4)	0.021256 ±4.0E-5	212.7 ±0.4 (397)	
-1.0[e]	—	—	—	-0.002146 ±4.0E-5	214.7 ±4.0 (4)	

[a] Read as 2.121×10^{-4}.

[b] one standard deviation

[c] $k(0)=0.999516\pm0.000028$

[d] Relative figure of merit with respect to "β_{eff} by Eq. (18) and a = 0.5"

[e] "prompt method"

Table7

Table 7 2-group constants for Λ calculation.

	Inner region	Outer region
D_1(cm)	1.4529	0.90541
D_2(cm)	0.19718	0.12565
Σ_{f1} (cm^{-1})	0.0026803	—
Σ_{f2} (cm^{-1})	0.064620	—
Σ_{a1} (cm^{-1})	0.0096419	0.00046006
Σ_{a2} (cm^{-1})	0.11741	0.018881
$\Sigma_s^{1\to2}$ (cm^{-1})	0.022521	0.058421
$\Sigma_s^{2\to1}$ (cm^{-1})	0	0
ν_p	2.3832	—
ν_d	0.0168	—
χ_1^p	0.98	—
χ_2^p	0.02	—
χ_1^d	0.5	—
χ_2^d	0.5	—
υ_1 (cm/s)	2.8×10^7	2.8×10^7
υ_2 (cm/s)	3.0×10^5	3.0×10^5

Table8

Table 8 Comparison of Λ by three methods.

c	Re[$\tilde{k}(c)$]	Im[$\tilde{k}(c)$]	Λ (s) by Eq. (47)	Λ (s) by Eq. (41)	Λ (s) by Eq. (40)
0	0.987184	0	—	—	2.7610E-5
10	0.987184	-2.6907E-4[a]	2.7610E-5	2.7634E-5	
30	0.987183	-8.0721E-4	2.7610E-5	2.7594E-5	
120	0.987167	-3.2287E-3	2.7610E-5	2.7561E-5	
240	0.987119	-6.4566E-3	2.7610E-5	2.7514E-5	
400	0.987004	-1.0758E-2	2.7610E-5	2.7454E-5	
500	0.986904	-1.3443E-2	2.7610E-5	2.7417E-5	
1000	0.986071	-2.6826E-2	2.7610E-5	2.7244E-5	

[a] Read as -2.6907×10^{-4}

Table9

Table 9 Comparison of Λ by Eq. (47) and Eq. (41) with the exact one (UO_2 fuel rod array)

c	Re[$\tilde{k}(c)$]	Im[$\tilde{k}(c)$]	Λ (s) by Eq. (47)	$1/k(c)-1/k(0)$ [c]	Λ (s) by Eq. (41)	Λ (s) by DANTSYS
20	1.001617 ±0.000056	-7.669E-4[a] ±2E-7[b]	3.822E-5 ±7E-9 (7E+4)[d]	—	—	3.832E-5
40	1.001516 ±0.000057	-1.534E-3 ±2E-7	3.823E-5 ±5E-9 (1E+5)	-1.537E-3 ±3.5E-5	3.842E-5 ±8.9E-7 (1)	
80	1.001519 ±0.000056	-3.067E-3 ±3E-7	3.823E-5 ±4E-9 (3E+5)	-2.988E-3 ±3.6E-5	3.735E-5 ±4.5E-7 (4)	
100	1.001383 ±0.000056	-3.834E-3 ±4E-7	3.824E-5 ±4E-9 (3E+5)	-3.786E-3 ±3.6E-5	3.786E-5 ±3.6E-7 (6)	
200	1.001423 ±0.000058	-7.667E-3 ±6E-7	3.823E-5 ±3E-9 (3E+5)	-7.637E-3 ±3.6E-5	3.818E-5 ±1.8E-7 (30)	

[a] Read as -7.669×10^{-4}.

[b] one standard deviation

[c] $k(0)=1.001502\pm0.000025$

[d] Relative figure of merit with respect to "Λ (s) by Eq. (41) and c = 40"

Table10

Table 10 Comparison of Λ by Eq. (47) and Eq. (41) with the exact one (Pu metal)

c	Re[$\tilde{k}(c)$]	Im[$\tilde{k}(c)$]	Λ (s) by Eq. (47)	$1/k(c)-1/k(0)$ [c]	Λ (s) by Eq. (41)	Λ (s) by DANTSYS
300	0.999505 ±0.000063	-3.510E-4[a] ±1E-7[b]	1.171E-6 ±4E-10 (3E+5)[d]	—	—	1.178E-6
500	0.999504 ±0.000063	-5.845E-4 ±2E-7	1.170E-6 ±4E-10 (3E+5)	-6.399E-4 ±4.9E-5	1.280E-6 ±9.7E-8 (1)	
1000	0.999501 ±0.000064	-1.169E-3 ±4E-7	1.170E-6 ±4E-10 (3E+5)	-1.176E-3 ±4.9E-5	1.176E-6 ±4.9E-8 (4)	
2000	0.999514 ±0.000062	-2.339E-3 ±7E-7	1.170E-6 ±4E-10 (3E+5)	-2.390E-3 ±4.9E-5	1.195E-6 ±2.4E-8 (13)	
4000	0.999366 ±0.000063	-4.676E-3 ±2E-6	1.170E-6 ±4E-10 (3E+5)	-4.613E-3 ±4.9E-5	1.153E-6 ±1.2E-8 (61)	

[a] Read as -3.510×10^{-4}.

[b] one standard deviation

[c] $k(0)=0.999565\pm0.000034$

[d] Relative figure of merit with respect to "Λ (s) by Eq. (41) and c = 500"